J. Astrophys. Astr. (2023)44:3
https://doi.org/10.1007/s12036-022-09895-8

Effects of initial ion velocity, magnetic field and plasma density profiles in simulating the plasma plume in a Hall thruster

SUKHMANDER SINGH[1,*] and HITENDRA K. MALIK[2]

[1]Department of Physics, Central University of Rajasthan, Kishangarh 305817, India.
[2]Plasma Waves and Particle Acceleration Laboratory, Department of Physics, Indian Institute of Technology Delhi, New Delhi 110016, India.
Corresponding author. E-mail: sukhmandersingh@curaj.ac.in

MS received 10 December 2021; accepted 12 September 2022

Abstract. Hall thrusters have high thrust-to-power ratio, efficiency and specific impulse. Therefore, less propellant mass is required for small satellite missions compared to chemical thrusters. In electric propulsion technology, the thrust is generated by the acceleration of ions in a cross-field plasma configuration. The fast ion bombardment near the exit channel is the main cause of erosion of the walls, which limits the lifetime of Hall thruster. The magnetic field profile controls the exhaust-beam divergence, motion of the energetic particles from the plume and erosion of outer surface of the device, which affects performance of the thruster. So, it is necessary to study the effect of different profiles of the magnetic field and density, and ion velocity on the plasma plume in addition to the impact of collisions between the plasma species. In this paper, we have investigated these effects on the plasma plume potential by considering Gaussian and super-Gaussian profiles for the density. The plasma plume is found to acquire larger potential, if the magnetic field of higher strength is used. The potential of the plasma plume attains a peak value outside the acceleration channel. The peak of the plume potential gets shifted more outside in the case of Gaussian density profile when the position of the magnetic field peak is shifted towards the cathode.

Keywords. Plasma plume—Hall thrusters—erosion—magnetic field profile—density gradient—efficiency—performance.

1. Introduction

Hall thrusters (HTs) are electrical propulsion devices having high specific impulse rather than chemical thrusters and used on spacecraft for a deep space mission, control the position of satellite, etc. This device generates propulsion by ejecting accelerated ions produced in a quasi-neutral plasma. The propellant, xenon is ionized inside a cylindrical channel and then, accelerated by electrostatic forces to create a propulsive thrust (Hagelaar *et al.* 2002; Mazouffre 2016; Boeuf 2017; Levchenko *et al.* 2018). The electric field is created by injecting electrons from a cathode situated at the exit of the channel and applying them to a radial magnetic field inside the channel that forces the electrons to stay for a long time inside the channel to get more ionization of the propellant. To overcome the space charge problems, in the exit side of the device, the ion beam is neutralized by the electrons generated from the external cathode, thus maintaining quasi-neutrality within the plasma plume (Hagelaar *et al.* 2002; Mazouffre 2016; Boeuf 2017; Levchenko *et al.* 2018). An azimuthal moving electron works as a virtual cathode. The ions continue their journey through the virtual cathode. Thus, the main source of the plasma plume of the Hall thrusters is the exhaust beam generated by the ionization of propellant. This plasma plume carrying high energetic particles that continuously bombarding the outer surface of the device as well as near any other objects in the space. These energetic particles reach to the surface of the device with a high velocity which may produce torque, heat flow, wall erosion, impurity and

This article is part of the Special Issue on "Waves, Instabilities and Structure Formation in Plasmas".

Published online: 16 January 2023

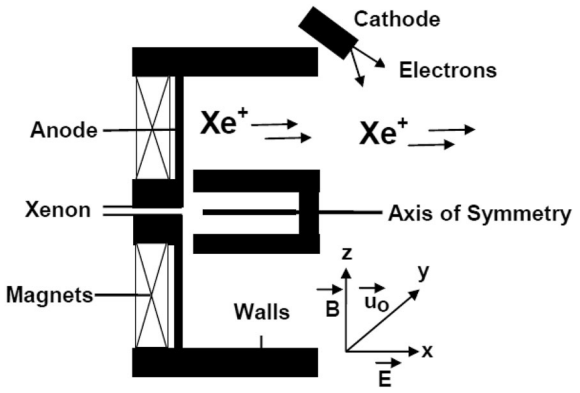

Figure 1. Hall thruster (cross-section view) schematic showing the crossed electric and magnetic fields.

electromagnetic interference (Hu & Wang 2015; Tyagi *et al.* 2018a, b; Malik *et al.* 2019). In addition, the flux of high energy and high amplitude of ions strike back towards the spacecraft, which may cause interference problems with solar panels and electronic instruments. Therefore, it is very important in designing the optimum magnetic field profiles to control the direction of plasma plume, erosion of the walls and performance of Hall thrusters (Chu *et al.* 2017). The schematic of a Hall thruster is shown in Figure 1.

Different theoretical studies were made to understand the potential inside a laboratory-model Hall thruster for two discharge current conditions and the study provides crucial information concerning the acceleration region of the thruster (Haas & Gallimore 2001). It has been seen that the potential remains nearly constant over the first 75% of the discharge channel and it drops to zero at the exit side of the plane. The effect of magnetic field gradient on the potential distribution in the presheath has been simulated by Keidar & Boyd (2005). They found that the length of the presheath decreases with increase in the magnetic field gradient and the potential drops to half, when the $(1/B)(dB/dx)$ increases from 0 to 0.5. They also theoretically investigated that the plasma potential substantially increases with the distance from the thruster exit (Keidar & Boyd 1999). The plasma potential is about 210 V (at 1 m from the thruster exit) and 125 V when the magnetic field is zero and 0.1 T, respectively.

Fruchtman *et al.* (2001) have shown theoretically to control the electric-field profile in the Hall thruster through the positioning of an additional electrode along the channel, which enhances the efficiency from 28% to 45%. The effect of the three magnetic field configurations on the plasma potential, plasma density and electron temperature were measured experimentally and theoretically by Dorf *et al.* (2006). It is seen that the electron temperature does not show strong dependence on the change of the magnetic field configurations as shown by plasma density (quadrupled) and plasma potential (doubled). Hofer *et al.* (2001) showed that the performance of the Hall thruster can be enhanced by reducing the divergence of the plume and the plume focal length can be enlarged to 100 cm. It is also demonstrated that thrust is higher, when thruster is working two-stage mode compared to a single-stage operation. Tumuklu & Levin (2018) did simulations and studied the effect of incoming free-stream ambient atomic oxygen direction on the ion thruster plume at 185 km and 300 km altitudes by varying the plume angle corresponding to the satellite orientation change in the orbit. It was perceived that the atomic oxygen affects the backflux of Xe at the lower altitude and the effect disappears at the altitude of 300 km. Karadag *et al.* (2018) experimentally designed external discharge plasma thruster (XPT) to design an efficient thruster. The electron density measurement was done with the ionization mean free path analysis. Faraday probe measurements showed that the plumes have Gaussian distributions. The higher electron density in the ionization region justifies the higher efficiency of XPT. Fruchtman & Cohen-Zur (2006) have analyzed the effect of magnetic field curvature on the plume divergence in the Hall thruster at the limit of zero electron pressure and derived the theoretical expression for the plume divergence in terms of magnetic field curvature. They concluded that the application of an additional emitting electrode can reduce plume divergence. Recently, Malik *et al.* (2021a, b, c) have shown that the plume divergence can be controlled by manipulating the magnetic field topology. Based on the magnetic field topology created by the tapered coils, a concept of plasma detachment in the plume has also been given by Malik (2022).

Morozov & Lebedev (1980) proposed to use a magnetic field lens to focus the plasma beam. Morozov *et al.* (1997) have designed a lens-type magnetic field with a zero magnetic point to make the plume divergence half angle only (10°) in SPT-ATON Hall thruster and observed experimentally that the amplitude of the low-frequency current oscillations of 10–20 kHz decreases, when the zero magnetic field is realized inside the channel.

Many new computational models have been developed using kinetic PIC simulations to evaluate the plasma properties inside Hall thrusters (Taccogna *et al.* 2008, 2019). The near-field plasma plume region has been simulated by Choi *et al.* (2009) with hybrid particle-fluid PIC-DSMC model for a D55 anode layer Hall thruster. The plasma was found to have a potential of 80 V (at 10 mm from the thruster exit) and 60 V, in the absence and presence of the magnetic field, respectively.

In the present work, we analyze the possible influence of the varying magnetic field and plasma density profiles (Gaussian and super Gaussian) on the plasma plume potential distribution in the exhaust from the Hall thruster within the framework of a quasi-one-dimensional free plasma jet model. The predicted results are compared with available experimental and simulation data and are found to be in good agreement. Along the magnetic field, the plasma potential is distributed according to the Boltzmann equilibrium. The different proposed profiles may be useful to design the efficient Hall thruster devices. Therefore, if the magnetic field and plasma density profiles are known from the experiments, then the plasma potential can be calculated.

The basic plasma model is given in Section 2. The optimum profiles of magnetic field and plasma density are proposed in Section 3. Computational domain and boundary conditions are given in Section 4. In Section 5, the differential equation is solved numerically to obtain the plume potential of the Hall thruster under the different configurations of profiles. The discussion is given in Section 6.

2. Basic fluid equations

Let us consider two component Hall thruster plasma with ions and electrons immersed in a magnetic field, which is pointing along the radial direction $\vec{B}(= B\hat{z})$ in the slab geometry. The electric field $\vec{E}$ is applied along the x-axis (axis of the thruster). The electrons rotate along the y-axis (azimuthal direction) because of the $\vec{E}\times\vec{B}$ drift. We take into account the collisions between the ions, electrons and neutrals. Further, considering the steady-state situation, below, we write the basic fluid equations for the ion and electron fluids along with constant rate of ionization.

$$\vec{\nabla}\cdot(\vec{v}_\alpha n_\alpha) = 0, \tag{1}$$

$$Mn_i(\vec{v}_i\cdot\vec{\nabla})\vec{v}_i = en_i\vec{E} - \vec{\nabla}p_i - Mn_iv_c\vec{v}_i + n_iv_{ie}m(\vec{v}_e - \vec{v}_i), \tag{2}$$

$$0 = -en_e\vec{E} - en_e(\vec{v}_e\times\vec{B}) - \vec{\nabla}p_e - n_ev_{ei}m(\vec{v}_e - \vec{v}_i) - n_evm\vec{v}_e. \tag{3}$$

In the above equations, n_i is ion density, M is ion mass, $\vec{v}_i$ is ion fluid velocity, $\vec{E}$ is axial electric field, n_e is electron density, m is electron mass, $\vec{v}_e$ is electron fluid velocity, v_{ei} is electron–ion collision frequency, v_c is ion charge exchange collision frequency and v is electron neutral collisions. Further, $p_i = Y_in_iT_i$ and $p_e = Y_en_eT_e$ together with T_i (T_e) as the ion (electron) temperature and $Y_i(Y_e)$ as the corresponding ratio of specific heats. n_α stands for n_i or n_e corresponding to $\alpha = i, e$ for the ions and electrons, and v_α stands for the velocity of the ions or electrons. Under this situation, taking into account that the magnetic field is perfectly parallel to the z-direction, only the x- and y-components of the particle velocity appear in the system of equation of motion. Hence, the above set of equations read as:

$$\frac{d(v_{\alpha x}n_\alpha)}{dx} = 0, \tag{4}$$

$$Mv_{ix}\frac{dv_{ix}}{dx} = eE_x - \frac{Y_iT_i}{n_i}\frac{dn_i}{dx} - Mv_cv_{ix} + mv_{ie}(v_{ex} - v_{ix}), \tag{5}$$

$$Mv_{ix}\frac{dv_{iy}}{dx} = mv_{ie}(v_{ey} - v_{iy}) - Mv_cv_{iy}, \tag{6}$$

$$0 = -\frac{eE_x}{m} - \frac{Y_eT_e}{mn_e}\frac{dn_e}{dx} - \frac{eB}{m}v_{ey} - vv_{ex} - v_{ie}(v_{ex} - v_{ix}), \tag{7}$$

$$0 = \frac{eB}{m}v_{ex} - vv_{ey} - v_{ei}(v_{ey} - v_{iy}). \tag{8}$$

By combining Equations (5) and (7), i.e., the equations for the plasma flow velocity in the axial direction, we get:

$$\frac{dv_{iy}}{dx} = \frac{v_{ei}}{v_{iy}}\frac{m}{M}\left(\frac{v_{ei}v_{iy} + \eta\omega_ev_{ix}}{v_{ei} + v}\right) - \left(\frac{m}{M}v_{ei} + v_c\right). \tag{9}$$

Here, we have introduced $v_{ex} = \eta v_{ix}$ by using the quasi-neutrality condition $(n_e = n_i)$ and Equation (4). Further, defining

$$\sqrt{\frac{Y_eT_e + Y_iT_i}{M}} \equiv C_s,$$

we obtain:

$$\left(C_s^2 - v_{ix}^2\right)\frac{dv_{ix}}{dx} = \left(\frac{m}{M}v\eta + v_c\right)v_{ix}^2 + \omega_iv_{ix}\left(\frac{v_{ei}v_{iy} + \eta\omega_ev_{ix}}{v_{ei} + v}\right), \tag{10}$$

$$\frac{d\varphi}{dx} = \frac{Y_e T_e}{e}\frac{d}{dx}\ln n(x) + \frac{m}{e}\upsilon_{ix}[\eta(\nu_{ei}+\nu) - \nu_{ei}] + B(x)\left(\frac{\nu_{ei}\upsilon_{iy} + \eta\omega_e\upsilon_{ix}}{\nu_{ei}+\nu}\right). \quad (11)$$

According to the model of Keidar & Boyd (1999), all the variables vary only along the axial direction, i.e., $\upsilon_{ix} = \upsilon_{ex}$ ($\eta = 1$) and $\upsilon_{iy} = 0$. Further, neglecting the collisions between the electrons and neutrals ($\nu = 0$), Equation (11) reduces to Equation (9) of Keidar & Boyd (1999). This way, Equation (11) reduces into the following form:

$$\frac{d\phi}{dx} = \frac{Y_e T_e}{e}\frac{d}{dx}\ln n(x) + B(x)\frac{\omega_e}{\nu_{ei}}\upsilon_{ix}. \quad (12)$$

The numerical solution of the above equation will give rise to the plasma plume potential for the different configurations of the plasma density and magnetic profiles. For the situation, when the magnetic field is zero, this equation reduces to the Boltzmann relation. Similar to the case of small density gradient and high magnetic field, Equation (12) represents the potential distribution in the ambipolar plasma flow across a magnetic field.

3. Proposed profiles of plasma parameters

To estimate the potential ϕ of the plasma plume, we assume particular profiles for the magnetic field and density, as earlier investigators (Fruchtman *et al.* 2001; Dorf *et al.* 2006) also noticed the importance of the same. It has been realized from various experiments that for a good operation of the thruster, the magnetic field should be large only in the exhaust region (Boeuf & Garrigues 1998; Ahedo & Escobar 2004). Hence, the axial profile of the magnetic field has taken the form of Equation (13), where B_m is maximum strength of the magnetic field and d is channel length.

Magnetic field profile:

$$B(x) = B_m \exp\left(-\frac{(x-g_B)^2}{d^2}\right). \quad (13)$$

This kind of magnetic field profile is shown in Figure 2, where its peak value can be tuned based on the parameter g_B. For example, the peak can be shifted towards the exit of the Hall thruster channel for the larger values of g_B. Similar axial distribution of the radial magnetic field has been considered by Boeuf & Garrigues (1998) for the simulations of the SPT 100 and SPT 50. Guerrini *et al.* (1998) designed SPT-50 thruster and have shown the comparison between the calculated and the measured radial components of the magnetic field on the thruster channel axis.

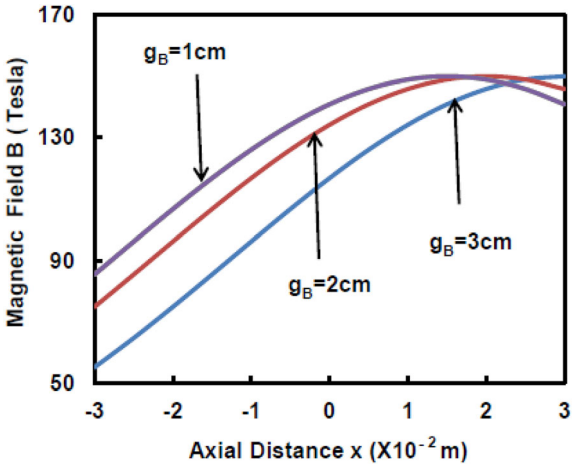

Figure 2. Three different profiles for the magnetic field, when $B_m = 145$ G and $d = 6$ cm.

In view of the larger gradient in the magnetic field at the entry region of the thruster channel (chamber) and the exit, this is plausible that the magnetized electrons will populate more almost in the middle region of the chamber. This is also justified because the plasma density would be maximum in the middle of the channel, as its generation takes place towards the anode at one end of the channel and neutralization of the ions occurs towards the other end, i.e., the exit of the thruster (Malik *et al.* 2019). Hence, the Gaussian distribution of the electron density seems to be the basic distribution in the chamber (Gallian *et al.* 2013). This is also supported by different magnitudes of the $\vec{E}\times\vec{B}$ drift in regions of different magnetic fields. Moreover, this is because the electrons spend more time in the region of higher magnetic field due to their larger gyrofrequency. Since the density of the electrons cannot show a sharp decay from the middle, this is appropriate to assume a broadened peak of this distribution that may correspond to the super-Gaussian distribution. Hence, in the present work, we have chosen both kinds of electron density distributions, i.e., the Gaussian distribution as shown in Equation (14) and the super-Gaussian distribution as shown in Equation (15) for a better comparison and to have a deep insight of the mechanism. Here, it would also be worth mentioning that the simulations conducted by Boeuf & Garrigues (1998) and other studies (Hofer *et al.* 2007, Kronhaus *et al.* 2012), which conclude that larger chances are there for the plasma density profile to attain almost similar shape as the magnetic

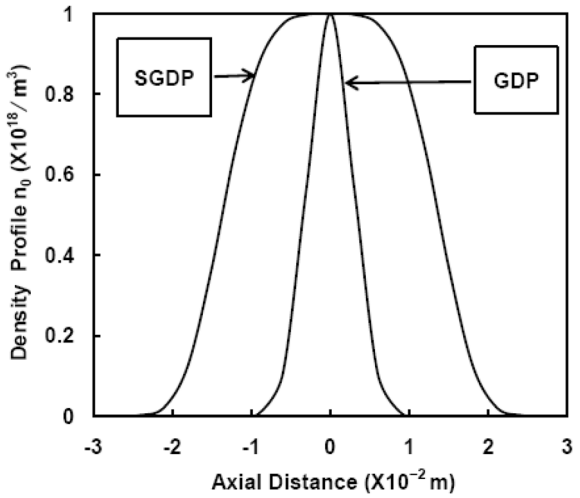

Figure 3. Two different profiles of the density, when $n_{0\max} = 1 \times 10^{18}$ m^3 and $d = 6$ cm.

field. However, this is expected to be modified in view of the electrons being injected into the chamber from the virtual cathode. On the other hand, the electron energy distribution function (EEDF) tends towards a super-Gaussian form in laser-produced plasma due to Langdon effect (Langdon 1980; Matte *et al.* 1988), when the inverse bremsstrahlung heating rate exceeds the electron thermalization rate (Milder *et al.* 2020). After having this detailed discussion, we select the following distributions for the electron density:

$$n_0(x) = n_{0\max} \exp\left[-15\left(\frac{x}{d}\right)^2\right], \tag{14}$$

$$n_0(x) = n_{0\max} \exp\left[-4\left(\frac{x}{d}\right)^4\right]. \tag{15}$$

Here, $n_{0\max}$ is the peak value of the density. These two types of electron density profiles, namely Gaussian profile (marked as GDP) and super-Gaussian profile (marked as SGDP), are shown in Figure 3, where $x = 0$ corresponds to the middle of the chamber.

4. Computational domain and boundary conditions

Field boundary condition is required for computing the Hall thruster plume, as shown in Figure 4. The upper boundary represents the wall, while the bottom boundary extends into the quasi-neutral bulk plasma region. The computation domain (starting at $x = -d/2$ cm and ending at $x = d/2$) allows us to resolve the Debye length and hence, compute the

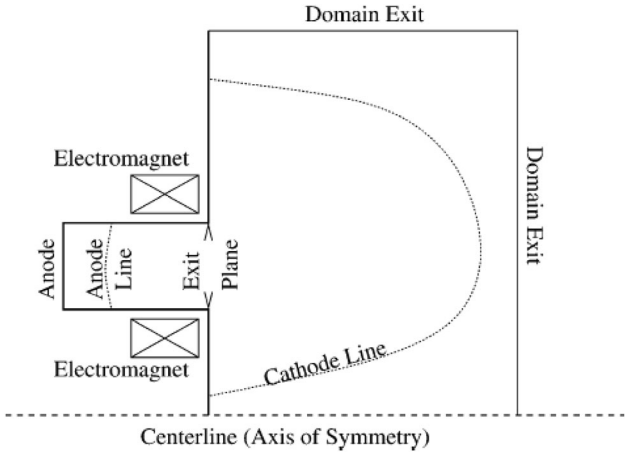

Figure 4. Hall thruster schematic: computational domain and boundary conditions.

potential by solving the Poisson's equation. The propellant is injected uniformly in the anode plane and their transport can be described by a simplified 1-D fluid equation. The anode and the primary ionization zone are located to the left. The domain captures the acceleration region characterized by the presence of strong applied magnetic field (Koo & Boyd 2004; Brieda & Keidar 2012).

5. Results and discussion

We numerically solve Equations (9)–(11) using Runge–Kutta method (Stanoyevitch 2011; Lindfield & Penny 2018) for the typical values of B_0, η, v_c, T_i, v, v_{ei}, v_{ix0}, v_{iy0} (Goebel & Katz 2008; Malik & Singh 2011, 2013; Singh & Malik 2011; Singh *et al.* 2013; Levko & Raja 2019; Samples & Wirz 2020) and T_e for examining the potential φ of the plasma plume (1-D case). However, the plume or the thruster channel can be simulated in detail (volumetric) using the computational fluid dynamics (Malik *et al.* 2021a, b, c; Malik & Tevatia 2021). In Figures 5 and 6, the dependence of the plume potential on the magnetic field is shown for the Gaussian density profile (GDP) and super-Gaussian density profile (SGDP), respectively. It is clear from Figure 5 that the potential (at $x = 3$ cm, exit point) is changed from 100 V to 130 V, when the magnetic field is increased from 135 G to 145 G. Keidaure & Boyd (1999) also observed that the potential of a plasma plume changes from -5 V to 25 V, when the magnetic field changed from zero to 0.1 T. In the case of SGDP (Figure 6), the maximum plume potential is increased from 70 V (at 12 cm) to 110 V (at 14 cm),

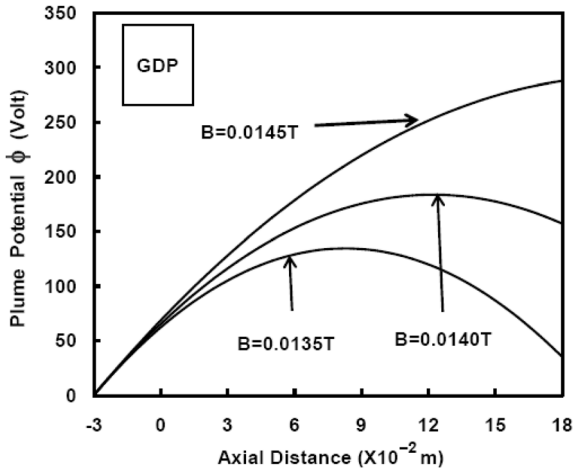

Figure 5. Dependence of plume potential φ on the magnetic field for Gaussian density profile in the plasma having X_e ions, when $T_e = 1$ eV, $B_0 = 200$ G, $T_i = 0.1$ eV, $n_0 = 10^{18}$ m^{-3}, $\upsilon_{ix0} = 300$ m s^{-1} and $\upsilon_{iy0} \sim 10$ m s^{-1}, $\nu_{ei} \sim 10^6$ s^{-1}, $\nu_c \sim 10^3$ s^{-1}, $\nu \sim 10^6$ s^{-1}, $\eta = 0.5$, $Y_e = 1$, $Y_i = 2$ and $\nu = 10^4$ s^{-1}.

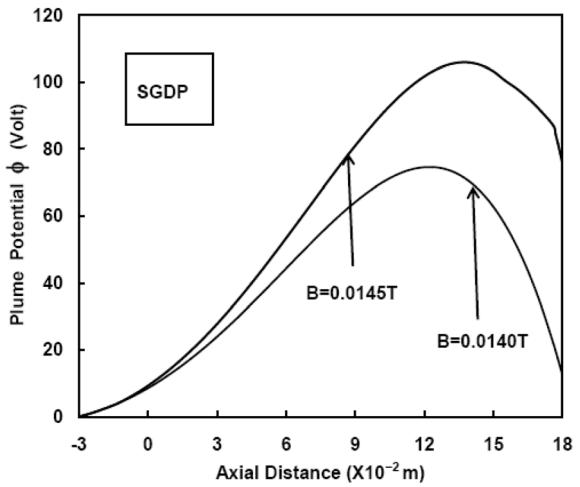

Figure 6. Dependence of plume potential φ on the magnetic field for super-Gaussian density profile for the same parameters as used in Figure 5.

when the magnetic field is varied from 140 G to 145 G. Similar observations were reported by Keidar & Boyd (1999) and others (Taccogna *et al.* 2008, 2019; Choi *et al.* 2009) for the variation of plume potential with the magnetic field.

The enhancement in the potential with the magnetic field can be understood in the following manner. In the present case, plasma jet enters a transverse magnetic field with a high supersonic directed velocity under the condition that the magnetic field is relatively weak so that only the electrons are magnetized,

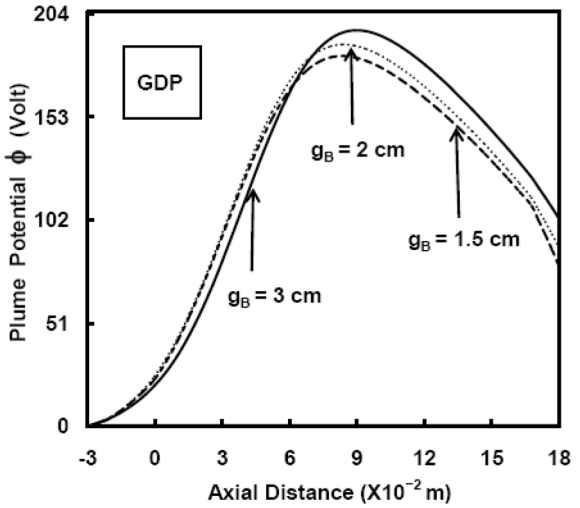

Figure 7. Dependence of plume potential φ on the position of magnetic field peak for Gaussian density profile for the same parameters as used in Figure 5.

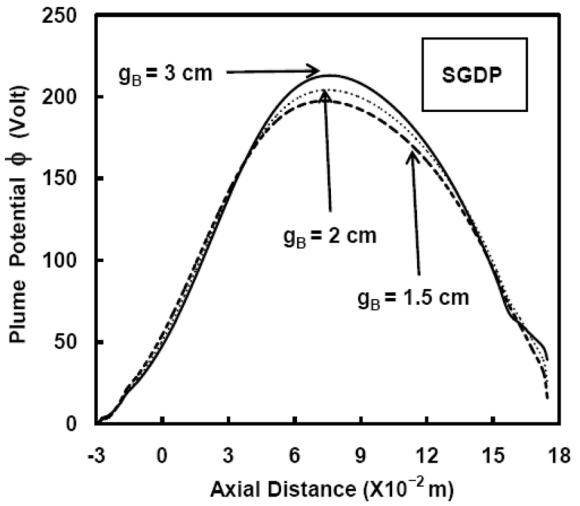

Figure 8. Dependence of plume potential φ on the position of magnetic field peak for super-Gaussian density profile for the same parameters as used in Figure 5.

whereas the ions move out of the effect of magnetic field. However, ambipolar current less plasma flow across the magnetic field may require an electric field to appear under the above condition. Therefore, we can expect the potential to increase across the magnetic field. On the other hand, it is seen from the figures that the plume potential attains a peak value outside the exit of the thruster, which was also observed by Keidar & Boyd (1999), Dorf *et al.* (2006) and Taccogna *et al.* (2008, 2019) in Hall thrusters.

The dependence of the plume potential on the position of the peak of magnetic field is shown in Figures 7 and 8 for both kinds of density profiles, i.e.,

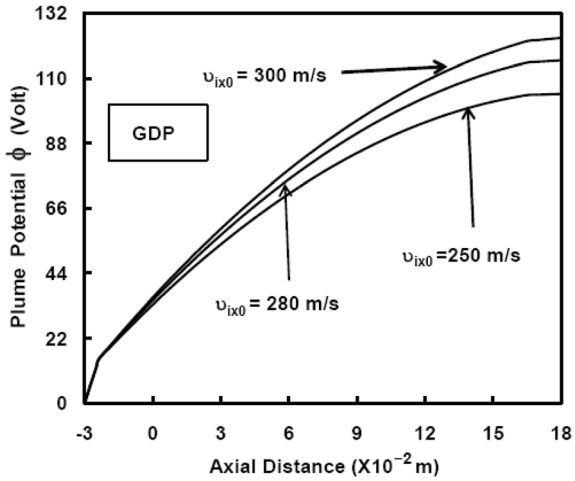

Figure 9. Dependence of plume potential φ on the initial axial ion velocity for Gaussian density profile for the same parameters as used in Figure 5.

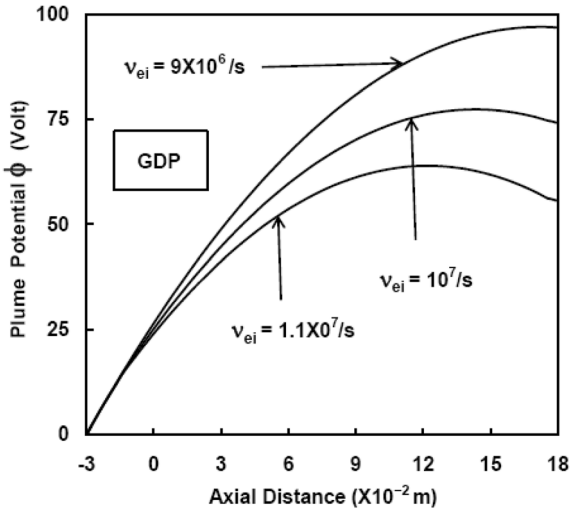

Figure 10. Dependence of plume potential φ on the electron−ion collision frequency for Gaussian density profile for the same parameters as used in Figure 5.

GDP and SGDP. It is apparent from Figure 7 that the peak of the plume potential gets shifted outside in the case of GDP, when the position of the magnetic field is shifted towards cathode and the peak potential is found to be 196 V (for $g_B = 3$ cm) and 183 V (for $g_B = 1.5$ cm). These findings are in agreement with the experimental and theoretical results reported by Dorf *et al.* (2006), where the effect of the magnetic field configuration was observed on the anode fall in a Hall thruster.

On the other hand, no shifting of the peak of the plume potential is observed if the density distribution is taken as super-Gaussian in the channel (Figure 8). However, the potential is increased to 213 V for $g_B =$ 3 cm and 198 V for $g_B = 1.5$ cm. This is due to the weak density variation in the plasma of the acceleration channel. Since the density acquires maximum value for a small region in the channel in the case of GDP, the nonuniformity in the density is significant and hence, a smooth distribution of the cyclotron motion of the electrons is not realized in the channel. Finally, this leads to shifting of the peak of the plume potential in the case of GDP. It can be seen that the predicted results are in agreement, which were observed experimentally and theoretically by Dorf *et al.* (2006). Similar plasma potential profile has also been predicted by Taccogna *et al.* (2008, 2019) in the kinetic simulations of plasma Hall thrusters.

The effect of initial axial velocity of the ions on the plume potential for the case of GDP is shown in Figure 9. Here, it is evident that the potential of the plume gets enhanced if the ions have larger initial axial velocity. It is increased from 53 V (for the case of 250 m s^{-1} velocity) to 58 V (for the case of 300 m s^{-1} velocity), when measured at the axial position of $x = 3$ cm, i.e., the exit. King *et al.* (1998) also reported the effects of plasma velocity on the plasma plume of an SPT-100 Hall thruster. On the other hand, in Figure 10, we have shown the dependence of the plume potential on the collision frequency between the ions and electrons. When the potential measured on the axial position ($x = 3$ cm), it falls to 40 V at larger collision frequency of 1.1×10^7 s^{-1} from 48 V at the collision frequency of 9.1×10^6 s^{-1}. This is obvious, as the larger collisions between the ions and the electrons lead to higher probability of recombination that may cause the lower potential of the plasma plume. These results are in agreement with an experiment by Keidar & Boyd (1999). However, insignificant effect of collisions between the electrons and neutrals is observed on the potential of the plasma plume (figures not shown).

Finally, the effect of electron temperature on the potential of the plasma plume for the GDP is shown in Figure 11. Here, the plume potential increases from 83 V to 124 V, when the electron temperature increases from 1 eV to 2 eV. This finding is consistent to the theoretical result obtained by Keidar & Boyd (1999) for a Hall thruster. Interestingly, the peak of the potential also gets shifted towards anode for the larger thermal motion of the electrons (higher temperature). This is plausible as the probability of recombination gets lower in the case of higher electron temperature that may lead to larger potential of the plasma plume.

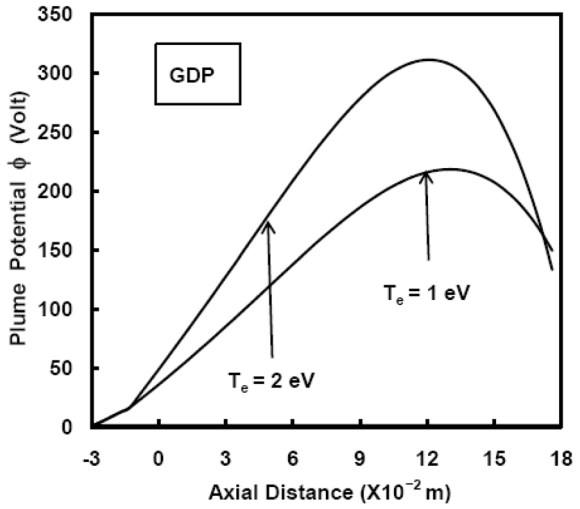

Figure 11. Dependence of plume potential φ on the electron temperature for the Gaussian density profile and the other parameters are same as in Figure 5.

6. Summary and conclusions

The effect of different profiles of the magnetic field and density was investigated on the plasma plume in addition to the influence of the ion velocity. Focus was given to the variation of potential of the plasma plume for which coupled equations were derived and solved numerically using Runge−Kutta method. The computation domain, starting at $x = -d/2$ cm and ending at $x = d/2$ (whereas potential is assumed to be zero) allowed us to resolve the Debye length and hence, could compute the potential by solving the Poisson's equation. Plasma plume is found to acquire larger potential if the magnetic field of higher strength is used. It is supposed that the nature of plasma potential is the result of magnetic field effects on the electron dynamics. In the region of plume field, the plasma flows across the magnetic field lines. Potential of the plasma plume attains a peak value outside the acceleration channel. The peak of the plume potential gets shifted more outside in the case of GDP, when the position of the magnetic field is shifted towards the cathode. No shifting of the peak of the plume potential is observed for the SGDP. Plume potential gets enhanced if the ions have larger initial axial velocity. Reduced potential of the plasma plume is realized for the higher frequency of the collisions of ions and electrons. The effect of electron temperature is found to enhance the potential of the plasma plume. The variation of plume potential with the electron temperature, initial axial velocity of the ions and electron–ion collisions are found similar for both types of plasma density profiles. These findings were compared with experimental and simulations studies conducted by other researchers. If the magnetic field and plasma density profiles are known from the experiments, the plasma potential can be calculated through the present proposal. Hence, the different proposed profiles may be useful to design the efficient Hall thruster devices.

Acknowledgments

The author SS appreciates the financial support given by the University Grants Commission (UGC), New Delhi, for providing the startup grant (Project No. F. 30-356/2017/BSR).

References

Ahedo E., Escobar D. 2004, J. Appl. Phys. 96, 983
Boeuf J. P. 2017, J. Appl. Phys. 121, 011101
Boeuf J., Garrigues L. 1998, J. Appl. Phys. 84, 3541
Brieda L., Keidar M. 2012, J. Appl. Phys. 111, 123302
Choi Y., Boyd I. D., Keidar M. 2009, J. Appl. Phys. 105, 013303
Chu Y., Han D., Cao Y., *et al*. 2017, Int. J. Numer. Anal. Model 14, 175
Dorf L., Raitses Y., Fisch N. J. 2006, Phys. Plasmas 13, 057104
Fruchtman A., Cohen-Zur A. 2006, Appl. Phys. Lett. 89, 111501
Fruchtman A., Fisch N. J., Raitses Y. 2001, Phys. Plasmas 8, 1048
Gallian S., Hitchon W. N. G., Eremin D., Mussenbrock T., Brinkmann R. P. 2013, Plasma Sources Sci. Technol. 22, 055012
Goebel D. M., Katz I. 2008, Fundamental of Electrical Propulsion of Ion Hall Thrusters (New York: Wiley)
Guerrini G., Michaut C., Bacal M., *et al*. 1998, Rev. Sci. Instrum. 69, 804
Haas J. M., Gallimore A. D. 2001, Phys. Plasmas 8, 652
Hagelaar G. J. M., Bareilles J., Garrigues L., *et al*. 2002, J. Appl. Phys. 91, 5592
Hofer R. R., Peterson P. Y., Gallimore A. D., *et al*. 2001, IEPC, 36
Hofer R., Mikellides I., Katz I., *et al.* 2007, XLIII AIAA/ASME/SAE/ASEE Joint Propulsion Conference (Cincinnati, OH), p. 5267
Hu Y., Wang J. 2015, IEEE Trans. Plasma Sci. 43, 2832
Karadag B., Cho S., Funaki I. 2018, J. Appl. Phys. 123, 153302
Keidar M., Boyd I. D. 1999, J. Appl. Phys. 86, 4786
Keidar M., Boyd I. D. 2005, Appl. Phys. Lett. 87, 121501
King L. B., Gallimore A. D., Marrese C. M. 1998, J. Propuls. Power 14, 327

Koo J. W., Boyd I. D. 2004, Comput. Phys. Commun. 164, 442
Kronhaus I., Kapulkin A., Balabanov V., *et al*. 2012, J. Phys. D: Appl. Phys. 45, 175203
Langdon A. B. 1980, Phys. Rev. Lett. 44, 575
Levchenko I., Keidar M., Xu S., *et al*. 2018, IEEE Trans. Plasma Sci. 46, 210
Levko D., Raja L. L. 2019, Plasma Res. Exp. 1, 035005
Lindfield G., Penny J. 2018, Numerical Methods: Using MATLAB. Academic Press
Malik L. 2022, Propulsion Power Res. 11, 171
Malik H. K., Singh S. 2011, Phys. Rev. E 83, 036406
Malik H. K., Singh S. 2013, Phys. Plasmas 20, 052115
Malik L., Tevatia A. 2021, Def. Sci. J. 71, 137
Malik H. K., Tyagi J., Sharma D. 2019, AIP Advances 9, 055220
Malik L., Escarguel A., Kumar M., Tevatia A., Sirohi R. S. 2021a, Laser Phys. Lett. 18, 086003
Malik L., Kumar M., Singh I. V. 2021b, IEEE Trans. Plasma Sci. 49, 2227
Malik L., Rawat S., Kumar M., Tevatia A. 2021c, Mater Today: Proc. 38, 191
Matte J. P., Lamoureux M., Moller C., *et al*. 1988, Plasma Phys. Control Fusion 30, 1665
Mazouffre S. 2016, Plasma Sources Sci. Technol. 25, 033002
Milder A. L., Le H. P., Sherlock M., *et al*. 2020, Phys. Rev. Lett. 124, 025001
Morozov A. I., Lebedev S. V. 1980, Rev. Plasma Phys. 8, 301
Morozov A. I., Bugrova A. I., Desjatskov A. V., *et al*. 1997, Plasma Phys. Rep. 23, 587
Samples S. A., Wirz R. E. 2020, Plasma Res. Express 2, 025008
Singh S., Malik H. K. 2011, IEEE Trans. Plasma Sci. 39, 1910
Singh S., Malik H. K., Nishida Y. 2013, Phys. Plasmas 20, 102109
Stanoyevitch A. 2011, Introduction to Numerical Ordinary and Partial Differential Equations Using MATLAB. John Wiley & Sons
Taccogna F., Schneider R., Longo S., *et al*. 2008, Plasma Sources Sci. Technol. 17, 024003
Taccogna F., Minelli P., Asadi Z., *et al*. 2019, Plasma Sources Sci. Technol. 28, 064002
Tumuklu O., Levin D. A. 2018, J. Spacecr. Rockets 55, 1154
Tyagi J., Sharma D., Malik H. K. 2018a, J. Theor. Appl. Phys. 12, 227
Tyagi J., Singh S., Malik H. K. 2018b, J. Theor. Appl. Phys. 12, 39